



HHS Public Access

Author manuscript

Mol Reprod Dev. Author manuscript; available in PMC 2023 August 01.

Published in final edited form as:

Mol Reprod Dev. 2022 August ; 89(8): 337–350. doi:10.1002/mrd.23626.

Borcs6 is required for endo-lysosomal degradation during early development

Charlotte J. Bell,

Neha Gupta,

Kimberly D. Tremblay,

Jesse Mager

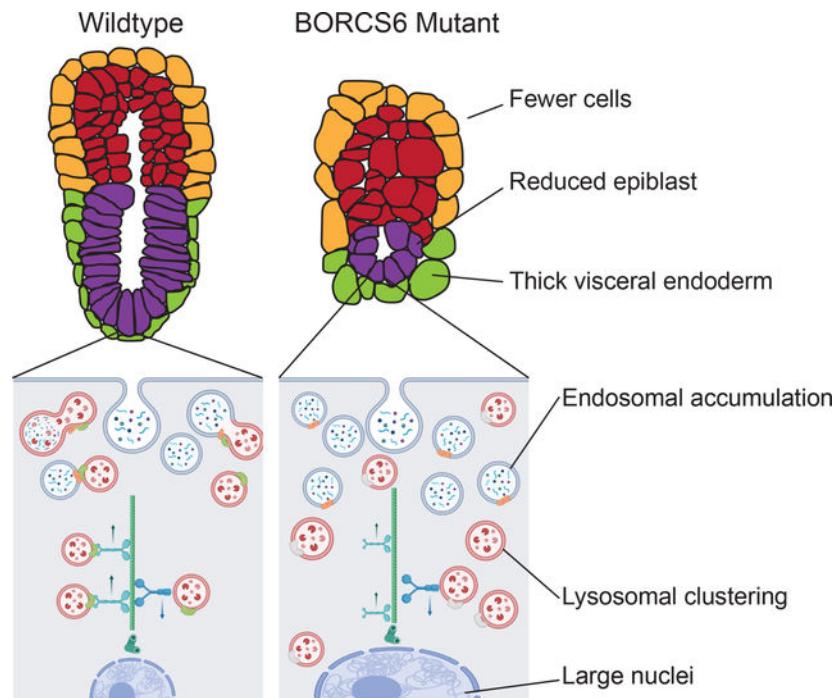
Department of Veterinary and Animal Sciences, University of Massachusetts, Amherst, MA, 01003, USA

Abstract

Early development and differentiation require precise control of cellular functions. Lysosomal degradation is a critical component of normal cellular homeostasis, allowing for degradation of signaling molecules, proteins, and other macromolecules for cellular remodeling and signaling. Little is known about the role of lysosomal function in mammalian embryos prior to gastrulation. Borcs6 is a protein involved in lysosomal trafficking as well as endo-lysosomal and autophagosome fusion. Here, we show that Borcs6 is necessary for efficient endo-lysosomal degradation in the early embryo. Although embryos lacking Borcs6 are developmentally comparable to control littermates at E5.5, they are characterized by large cells containing increased levels of late endosomes and abnormal nuclei. Furthermore, these embryos display a skewed ratio of extraembryonic and embryonic cell lineages, are delayed by E6.5 and do not undergo normal gastrulation. These results demonstrate the essential functions of lysosomal positioning and fusion with endosomes during early embryonic development and our results indicate that the early lethality of BORCS6 mutant embryos is primarily due to defects in the HOPS-related function of BORC rather than lysosomal positioning.

Graphical Abstract

Corresponding author: Jesse Mager; jmager@umass.edu.



Created with BioRender

Keywords

Borcs6; development; knockout; autophagy; lysosome

Introduction

Approximately five- and one-half days after fertilization (E5.5), the mouse embryo has formed a radially symmetric egg cylinder, with distinct epiblast, extraembryonic ectoderm, and visceral endoderm cell types. Approximately one day later, the embryo will begin gastrulation, the process by which the epiblast will differentiate into endoderm, ectoderm, and mesoderm. Before gastrulation is initiated, rapid proliferation occurs in the epiblast until enough cells have been produced to support and initiate gastrulation (Power and Tam, 1993). Gastrulation is a highly dynamic and carefully orchestrated series of morphogenetic events which defines the anterior-posterior axis within the embryo. The primitive streak initiates through an epithelial-to-mesenchymal transition of epiblast cells, followed by formation of the primitive node and establishment of the primary germ layers which later differentiate into organ progenitors. Successful gastrulation requires specific crosstalk between tissues of the embryo as well as establishment of several signaling gradients (Arnold and Robertson, 2009). Spatiotemporal control of these morphogen gradients is accomplished in part by degradation of signals through the endo-lysosomal pathway. Cellular memory of exposure to a morphogen can also be eliminated through lysosomal degradation of receptors, allowing for sensitive and rapid cellular responses (Jullian and Gurdon, 2005).

Lysosomes are found within every eukaryotic cell and are highly acidic membrane-bound organelles that contain digestive enzymes. Lysosomes are responsible for degradation of both intracellular and extracellular substances through fusion with endosomes and autophagosomes, respectively (Perera and Zoncu, 2016). Lysosomes have been shown to play significant roles in detoxification, metabolic signaling, and gene regulation (Ballabio and Bonifacio, 2020). During early embryonic development, autophagy (elimination of dysfunctional/unnecessary cells) is particularly important for proper function of the visceral endoderm (VE) which plays a critical role in nutrient uptake and delivery to the early embryo. Microautophagy, which involves lysosomal engulfment of whole endosomes containing small cytosolic components, has a unique role in the VE due to the presence of apical vacuoles, a specialized type of lysosome (Wada et al., 2013). Because the VE surrounds and covers the epiblast until gastrulation occurs, apical vacuoles engulf maternal nutrients and cytokines before they can enter future embryonic cells (the epiblast) (Wada, 2013). Furthermore, uptake and endocytosis of signaling molecules such as Nodal, Wnt, and BMPs into the apical vacuoles is crucial for embryonic patterning (Kawamura et al., 2012). Thus, the early embryo provides an important and informative model for understanding the impact of alteration or loss-of-function of lysosome-related genes.

Lysosomal breakdown of molecules requires three main events: lysosomes must be transported near endosomes, the membranes of both organelles must interact and fuse, and specific enzymes contained by the lysosome must break down the endosomal contents. For the first of these cellular events, lysosomes are transported between perinuclear and peripheral pools along microtubule tracks by distinct trafficking mechanisms (Matteoni and Kreis, 1987; Cabukusta and Neefjes, 2018). Cellular conditions such as pH or nutrient levels influence lysosomal distribution subsequently affecting lysosomal function and cellular signaling (Heuser, 1989; Korolchuk et al., 2011). The second step involves protein interactions between lysosomes and endosomes or autophagosomes, which trigger assembly of a SNARE protein complex. The final step, degradation, is mediated by over 60 hydrolases targeting specific molecules that are contained within lysosomes (Xu and Ren, 2015). Defects in any of these events can have devastating cellular and organismal consequences and can result in many well documented human disorders termed lysosomal storage diseases (LSD). The best characterized LSDs are those involving specific enzymatic deficiencies or dysfunctions. However, less is known about defects in the lysosomal transport and membrane fusion events, especially *in vivo* during early embryonic development.

BLOC-1 Related Complex (BORC) is a protein complex hypothesized to be involved in both lysosomal trafficking and fusion with endosomes (Pu et al., 2015; Jia et al., 2017). Although the BORC and BLOC-1 complexes share three subunits (BLOS1, BLOS2, and Snapin), but they are functionally distinct, with BLOC-1 responsible for biogenesis of melanosomes and platelet-dense granules (Falcon-Perez et al., 2002). In addition to the three shared subunits, BORC also contains BORCS4, BORCS5, BORCS6, BORCS7, and BORCS8 (Pu et al., 2015). Knockout models of BLOS1, BLOS2, Snapin, BORCS4, BORCS5, and BORCS7 have been examined in detail (Zhang et al., 2014; Zhou et al., 2016; Tian et al., 2005; Yang et al., 2012; De Pace et al., 2020; Snouwaert et al., 2018), and a knockout BORCS8 results in preweaning lethality (Dickinson et al., 2016). While each of these homozygous knockout phenotypes results in lethality, the timing varies greatly among subunits ranging from E9.5

though pre-weaning. However, the consequences of removing BORCS6 have not yet been investigated in a mouse model, providing an opportunity to better understand the role of BORC *in vivo*.

Lysosomes are transported towards and away from the nucleus along microtubule tracks by separate mechanisms. BORC is hypothesized to associate with the cytosolic face of the lysosome and is involved in the recruitment and activation of the GTPase Arl8 by acting as a guanine exchange factor, which in turn recruits the cofactor SKIP (Pu et al., 2015; Niwa et al., 2017). SKIP allows kinesin-1 or kinesin-3 to attach to lysosomes for movement along microtubules away from the nucleus. In addition to enabling lysosomal tethering to kinesin motor protein, Arl8b is known to recruit the HOPS complex (Khatter et al., 2015; Garg et al., 2011). The HOPS complex catalyzes assembly of SNARE complexes, enabling late endosomes or autophagosomes to fuse with lysosomes (Orr et al., 2017). Knockout models for several HOPS components have been analyzed. Most notably, knockout of mVam2 led to fragmented endosomal compartments and ectopic activation of BMP signaling in the early embryo, causing lethality around day 9 in mice (Aoyama et al., 2012). BORC is hypothesized to directly interact with HOPS to promote autophagosome-lysosome fusion (Jia et al., 2017). Thus, BORC may play an integral role in several processes necessary for proper lysosomal function, facilitating both lysosome trafficking and fusion with endosomes and autophagosomes.

Here we present *in vivo* analysis and characterization of embryos devoid of *Borcs6* function. Unlike other members of BORC, we show that BORCS6 is necessary for the initiation of gastrulation, and document severe defects in visceral endoderm and embryo patterning, as well as defects in function of the endo-lysosomal pathway.

Results

Expression of BORCS6

The *Borcs6* gene is comprised of only one exon. We used a knockout allele, *Borcs6*^{tm1.1(KOMP)Vlcg}, which was generated by the Jackson laboratory as part of the NIH sponsored Knockout Mouse Project (Dickinson et al., 2016). This allele replaces most of the *Borcs6* exon with a *lacZ* reporter construct. We first generated and collected heterozygous embryos at various stages and performed X-gal staining to identify the reporter gene expression pattern of *Borcs6*. In E3.5 heterozygous blastocysts, *lacZ*-positive staining was observed in both the inner cell mass (ICM) and trophoctoderm (TE), indicating widespread expression (arrows in Fig. 1A). Shortly after implantation at E4.5, *lacZ* is detected throughout the embryo, both in the trophoctoderm and in the ICM (Fig 1F). At E5.5, the extraembryonic ectoderm and visceral endoderm surrounding it show robust *lacZ* staining in both wholemount and section (Fig. 1B and G–G'), while the epiblast and distal half of the visceral endoderm show noticeably less staining, which could be indicative of either low expression levels or more likely perdurance of β -galactosidase leftover from expression at an earlier stage (Fig. 1G''). This pattern continues E6.5, with a further reduction in *lacZ* signal in the epiblast (Fig. 1C, H–H''). However, some staining remains in both the epiblast (Fig 1H'', arrowhead) and visceral endoderm (Fig 1H'', arrow) (Fig. 1C''). The expression pattern remains similar at E7.5, with *lacZ*-positive cells throughout the extraembryonic

ectoderm and visceral endoderm surrounding it (Fig. 1D and I-I'') and sparse staining throughout the epiblast (Fig. 1I'', arrowhead) and distal half of the visceral endoderm (Fig. 1I'', arrow). To confirm that the *lacZ* reporter faithfully recapitulates endogenous expression, we performed whole mount *in situ* hybridization (WISH) with a probe designed to recognize the normal *Borcs6* transcript and observed the same pattern of mRNA localization at E7.5 (Figure 1E). To summarize, *Borcs6* expression appears to be ubiquitous in blastocysts, but shows a marked reduction in the epiblast and visceral endoderm surrounding the epiblast at E5.5-E6.5.

Morphogenetic defects in *Borcs6*^{-/-} embryos

The International Mouse Phenotyping Consortium reported that mice homozygous for a null mutation of *Borcs6* were not found at birth (0/86) or at embryonic day E9.5 (0/29), indicating that *Borcs6* is critical for proper embryonic development beyond organogenesis stages (Dickinson et al., 2016). To produce mutant embryos, we performed timed mating of heterozygous *Borcs6* males and females and dissected embryos at various stages of development preceding E9.5.

At E7.5, homozygous *Borcs6* mutant embryos (hereafter referred to as “mutants”) are severely reduced in size with no discernable features of a normal E7.5 embryo (Fig. 2A). Abnormally large visceral endoderm (VE) cells are apparent, but the epiblast and extraembryonic ectoderm appear to have died, resulting in a very small E7.5 mutant (Fig. 2B–E). Despite the much smaller size of the mutant embryo at E7.5 (Fig. 2A), the Reichert’s membrane (RM) is comparable in size and expansion to wildtype embryos but with a large cavity between the RM and embryo (Fig. 2C, E). Homozygous *Borcs6* mutants were found at normal Mendelian ratios at E6.5 and E7.5 (21% mutant, 53% heterozygous and 26% wildtype embryos recovered, data not shown), indicating either that *Borcs6* is not required for blastocyst formation, implantation or initial egg-cylinder formation, or that maternal *Borcs6* RNA/protein is sufficient for these earliest stages of development. At E6.5, mutant embryos are similar in overall size to wildtype littermates (Fig. 2F) but present with a distinct phenotype. From a gross morphological perspective, the most striking feature of mutant embryos at E6.5 are very large cells in the distal half of the visceral endoderm (VE, arrowheads Fig. 2F). We performed RT-PCR to examine developmental markers at E6.5 including *Wnt3*, *Hhex*, *Eomes* and *Brachyury* (Fig. 2F'). Surprisingly we observed seemingly normal expression of each of these genes in mutant embryos at E6.5, suggesting that signaling and differentiation events in the early egg-cylinder (E5-E6) are not completely disrupted by the absence of *Borcs6* (Fig. 2F').

Because mutant embryos appear so abnormal at E7.5, we focused our phenotypic characterization on embryos at E6.5. We performed *in situ* hybridization to further examine expression of *Brachyury* as a marker of the nascent primitive streak. Although RT-PCR indicates expression of *Brachyury* in mutant embryos (Fig. 2F'), ISH results are variable. Some mutant embryos show no signal, while other mutants show some *Brachyury* with variable expression level and disorganized localization in consecutive sections (Fig. 2G). The difference among mutants may be due to either variation in developmental “age” from one mutant to the next or more likely may reflect the drastically reduced

epiblast population resulting in disruption of normal morphogenetic events leading up to gastrulation. Regardless, none of the 5 mutant embryos examined by ISH show robust *Brachyury* expression appropriately localized to the presumptive posterior of the embryo as seen in all control embryos (Figure 2G) indicating that while some mutants may initiate expression of *Brachyury*, there is no properly organized primitive streak at E6.5.

We next performed immunofluorescence to identify defects in morphology and overall organization. DAPI was used to stain the nuclei, and E-cadherin to mark epithelial cell-cell adhesion. Wildtype E6.5 embryos are composed of organized cells with uniformly sized nuclei in all lineages (Fig. 2J–J’). In contrast, mutant embryos have cells with obviously larger nuclei and lack epithelial organization (Fig. 2K–K’). We also used antibodies against *Cdx2* and *Oct4* to identify the extraembryonic ectoderm and epiblast, respectively. Although mutant extraembryonic ectoderm appeared similar in size and cell number to wildtype littermates, the mutant epiblast appeared much smaller with far fewer *Oct4*-positive cells (Fig. 2J’’–J’’’, 2K’’–K’’’). One possible explanation for fewer cells in our mutant embryos could be increased levels of apoptosis. We performed TUNEL staining on sectioned E6.5 embryos to examine cells undergoing apoptosis (Fig. 2L–M). Mutant E6.5 embryos have an average of 7 TUNEL-positive cells (N=3), while wildtype controls average only 1 TUNEL-positive cell (Figure 2J–K). Given the vastly reduced total number of cells in mutant embryos (see Fig. 3), there is a significant increase in percent apoptotic cells in *Borcs6* mutants ($p < 0.0001$). The apoptotic cells were distributed throughout mutant embryos, showing no elevated presence in any particular lineage (Fig. 2L–M).

To further characterize morphological differences between wildtype and mutant embryos at E6.5, we performed various quantitative measurements of paraffin embedded and sectioned mutant and wildtype embryos at E6.5 (Figure 3). Representative control and mutant embryos are shown in Figure 3A–D’, but a total of 12 control and 10 mutants were analyzed. The thickness of the visceral endoderm surrounding the extraembryonic ectoderm was not significantly altered in mutants. However, consistent with whole mount observations (Fig 2F), the visceral endoderm surrounding the epiblast was significantly thicker in mutant embryos than in control littermates ($P = 0.0012$, Fig. 3F). Additionally, when comparing cell area in the extraembryonic ectoderm and epiblast, cells of both ectodermal lineages are larger in the mutant embryos ($P < 0.001$, Fig. 3G). Nuclear areas are also significantly larger throughout the embryo in mutant embryos than control littermates ($P < 0.001$, Fig. 3H). In control littermate embryos the epiblast and extraembryonic ectoderm are similar in proximal-distal height, with an epiblast approximately 1.1 times longer than the extraembryonic ectoderm (Fig. 3I). In mutant embryos, the absolute height of the extraembryonic ectoderm does not differ significantly from controls (data not shown), but the epiblast is only half of the height of the extraembryonic ectoderm, resulting in a significantly change in the normal morphometric ratios ($P = 0.0016$, Fig. 3I).

To further understand the tissue-specific defects, we counted the total number of extraembryonic ectoderm and epiblast cells in mutant and control E6.5 embryos (Fig 3J). As expected, mutant embryos had fewer cells of both lineages as compared to control littermates, with a more drastic reduction of epiblast cells ($P < 0.05$). To confirm whether this was simply a result of developmental delay, we also compared mutant embryos to E5.5

control embryos. Although the number of extraembryonic ectoderm cells were comparable in mutant embryos and E5.5 controls, epiblast cells were still reduced in mutant embryos ($P < 0.05$), indicating lineage specific consequences due to loss of *Borcs6* function – while the extraembryonic lineages continue to proliferate, the epiblast does not. To summarize, mutant embryos are characterized by larger cells throughout, thicker distal half of the visceral endoderm, and greatly reduced epiblast size and cell number.

***Borcs6*^{-/-} embryos accumulate Rab7-positive late endosomes and fail to disperse lysosomes**

Due to the established role of BORCS6 in the endo-lysosomal pathway (Pu et al., 2015), we examined the distribution of endosomes and lysosomes in BORCS6 mutant embryos. We performed IF with antibodies against LAMP1 (a protein on the lysosomal membrane) and RAB7 (marks the surface of late endosomes) to visualize lysosomes and endosomes, respectively. In control littermate E6.5 embryos, both Lamp1 and Rab7 show faint signals throughout all cells, indicating the normal dispersal of these vesicles (Fig. 4C'–C''). Areas high in Lamp1 also show an elevation in Rab7, indicating endosomes and lysosomes are in close proximity, likely poised for endosomal degradation (Fig. 4C'''). In *Borcs6*-null embryos, large, discrete Rab7-positive vesicles are evident, suggesting an accumulation of late endosomes (Fig. 4D'). This accumulation occurs primarily in the mutant visceral endoderm (Fig. 4D'). Lamp1 signal is also stronger in mutant embryos and often with many foci grouped, suggesting lysosomal clustering rather than dispersal throughout the cells (Fig. 4D''). When examined together, Rab7 and Lamp1 often cluster separately (Fig. 4D'''). Taken together, these results support the hypothesis that loss of BORCS6 impacts both lysosomal positioning and proper degradation of late endosomes through fusion with lysosomes.

We also used whole-mount immunofluorescence followed by confocal imaging to better visualize endo-lysosomal compartments in whole cells throughout the visceral endoderm. Wildtype E6.5 embryos have higher levels of late endosomes and lysosomes in the proximal half of the visceral endoderm than in cells of the distal half (as indicated by Rab7 and Lamp1 signal, respectively (Fig. 4E–E'')). However, mutant embryos have late endosomes and lysosomes dispersed evenly throughout the visceral endoderm, with no obvious difference in the proximal versus distal parts of the visceral endoderm (Fig. 4F–F''). Careful analysis also revealed that Rab7 and Lamp1 signals overlap extensively in wildtype embryos, indicating colocalization of late endosomes and lysosomes (Fig. 4G), but mutant embryos show large discrete patches of Rab7 and Lamp1, suggesting a failure of lysosomes to be transported to endosomes for degradation of endosomes (Fig. 4H). Furthermore, the vesicles encapsulated by these membrane markers appear much larger and more densely packed in mutant cells (Fig. 4G, 4H), supporting the hypothesis that breakdown of vesicle contents is not occurring or is greatly defective in the absence of *Borcs6* function.

***Borcs6* is required for efficient degradation of endocytic vesicles**

In order to functionally test the ability of *Borcs6* mutant cells to degrade endocytic vesicles, we designed a pulse-chase style experiment with whole mount embryo culture in media containing a fluorescent dextran. As expected, after 10 minutes in culture with dextran-647

followed by a 10-minute chase in culture media alone, dextran-647 was found in small vesicles within the visceral endoderm for both wildtype and mutant embryos (Fig. 4I–I', 4J–J'). After the 10-minute chase, the dextran-647 appears with similar intensity between mutant and control littermates, suggesting that endocytosis occurs normally in mutant embryos. After 45 minutes, the dextran-647 in control embryos has been trafficked further into the embryo, with some signal seen in the proamniotic cavity (Fig. 4K), with apparent consolidation into larger vesicles (Fig. K'). However, in mutant embryos, the dextran was still found only in the visceral endoderm and remained in many small vesicles per cell (Fig. 4L–L'). After 65 minutes we fixed and counterstained embryos with DAPI. In control embryos, the vast majority of dextran-647 was degraded in the visceral endoderm, with few dispersed vesicles apparent in the normal epiblast (Fig. 4M–M'). In stark contrast, a large amount of dextran-647 was still observed in the mutant visceral endoderm in small, concentrated vesicles, suggesting that endosomes were not properly degraded in *Borcs6* mutant cells (Fig. 4N–N'). In addition, no dextran-647 was apparent in the mutant epiblast, further indicating defects in transport between mutant visceral endoderm and epiblast.

Discussion

In this study, we show that *Borcs6* is necessary for normal development prior to and during gastrulation stages (E5.5–6.5). While mutant embryos do show developmentally appropriate expression of some genes, *Borcs6*-null embryos fail to organize a primitive streak expressing *Brachyury* (Fig. 2E'–E'') or develop normal morphological features of gastrulation such as a node and allantois. Interestingly, compared to loss of function mutations in other components of BORC, including the components shared by BORC and BLOC-1 protein complexes, *Borcs6*-null embryos die earlier with a much more severe phenotype. *Blos1*-null mutant embryos are embryonic lethal at E12.5 (Zhang et al., 2014), while *Blos2* causes late embryonic or perinatal lethality when removed (Zhou et al., 2016) and *Snopin* knockouts are perinatal lethal (Tian et al., 2005). Mice lacking BORCS5 and BORCS7 die at birth (De Pace et al., 2020; Snouwaert et al., 2018), and mice lacking BORCS4 survive into adulthood (Yang et al., 2012). Although BORCS8 has not been investigated in detail, the IMPC has found that knockout mice show incomplete penetrance of preweaning lethality (Dickinson et al., 2016). Thus, we believe that BORCS6 plays a unique and critical role as part of the BORC complex that cannot be compensated for by other subunits, resulting in an earlier phenotype observed than for other BORC subunits.

As mentioned above, the BORC complex plays a role in both lysosomal trafficking and fusion with endocytic vesicles through interaction with the HOPS complex (Pu et al., 2015; Jia et al., 2017). Our data show clustering of lysosomes in BORCS6 mutants (Fig 4), suggesting a defect in trafficking mechanisms. Although lysosomes do not appear to be clustered around the nucleus as reported in BORCS6-deficient HeLa cells (Pu et al., 2015), Lamp1 signal appears significantly more dispersed in control littermates than in mutant embryos.

Borcs6-null cells have significantly larger nuclei than control embryos (Fig. 3H). Disruption of autophagy has been shown to decrease centrosome stability, causing defects in chromosome segregation, and resulting in larger than normal nuclei (Holdgaard et

al., 2019). Furthermore, RNAi-mediated depletion of ARL8B and SKIP, two proteins functioning downstream of BORC, have been shown to increase both mitotic errors such as chromosomal bridges and nuclear aberrations such as toroidal nuclei, suggesting that lysosomal positioning is critical for timely and accurate completion of mitosis (Almacellas et al., 2021). Although we do not observe an obvious increase in the number of mitotic cells in mutant embryos, the presence of abnormally large nuclei may indicate a failure to properly regulate and/or complete mitosis. These findings highlight the importance of BORC-mediated lysosomal trafficking and suggest a requirement of Borcs6 for progression through mitosis. Considering increased levels of TUNEL-positive cells found in mutant embryos (Fig. 2J–K), combined defects in mitosis plus increased apoptosis could certainly explain the drastically reduced number of cells in mutant embryos (Fig. 3J).

Our data also show that Borcs6-null embryos have larger cells in the extraembryonic ectoderm, epiblast, and visceral endoderm than control embryos (Fig. 3F, H). Disruption of lysosomal degradation has been shown to result in the accumulation of vesicle-like structures, presumably late endosomes, in the visceral endoderm (Aoyama et al., 2012). Immunofluorescence using Rab7 reveals elevated levels of late endosomes throughout Borcs6-null embryos, especially in the visceral endoderm. This increased cell size may be due to both increased cytoplasmic volume (due to inefficient degradation of endosomal contents) and larger nuclei. Another possible explanation for the increased cell volume could be a failure of cells to complete cytokinesis. Although we did not observe elevated numbers of cells positive for the mitotic marker phospho-H3 (data not shown), further experiments are needed to distinguish these possible explanations. It is also apparent that the visceral endoderm remains surrounding the epiblast and is not replaced or moved by any newly defined definitive endoderm in Borcs6-null embryos.

Proper function of the endocytic pathway requires that extracellular materials are first taken up in vesicles and delivered to early endosomes. Early endosomes then undergo a maturation process during which Rab5 is replaced by Rab7, membrane proteins change, luminal pH decreases, and morphology is altered (Huotari and Helenius, 2011). We observed comparable uptake of fluorescent dextran in wildtype and mutant embryos, suggesting that the initial steps of endocytosis occur normally without functional BORCS6. However, our data show that endocytosed dextran-647 remains sequestered in endosomes in the visceral endoderm of mutant embryos without being completely degraded as in controls. Furthermore, immunofluorescence reveals an accumulation of Rab7-positive late endosomes in mutant embryos. Taken together, these data suggest that in the absence of Borcs6 function, endosomes are capable of maturation but are unable to fuse with lysosomes for degradation.

Our data also show a dramatic reduction in the number of epiblast cells in E6.5 Borcs6 mutants. Although the mutant extraembryonic ectoderm cell numbers remain comparable to E5.5 control embryos, there are significantly fewer Oct4 positive mutant cells even when compared to E5.5 controls (Fig. 3J), suggesting an epiblast tissue-specific defect in Borcs6 null embryos. Importantly, mVam2 knockout embryos show a similar phenotype, with epiblast reduction, accumulation of late endosomes, and early embryonic lethality (Aoyama et al., 2012). mVam2 is a component of the HOPS complex, which interacts with

BORC to mediate fusion of lysosomes with endosomes or autophagosomes (Jia et al., 2017). Notably, mVam2 is the subunit recruited by Arl8b to assemble HOPS and has been shown to coprecipitate with BORCS6 (Garg et al., 2011; Jia et al., 2017). Therefore, a logical conclusion is that the severe phenotype seen in BORCS6 mutant embryos is primarily due to defects in the HOPS-related function of BORC rather than lysosomal positioning function. Aoyama et al., (2012) suggest that the patterning defect seen in mVam2 mutant embryos is due to inadequate endocytic downregulation of BMP signals near the epiblast, resulting in a skewed BMP4 gradient. It is highly likely that a similar mechanism is governing the phenotype seen in BORCS6 mutant embryos, with defects in lysosomal function inhibiting the termination of BMP4 signaling necessary to promote distal visceral endoderm differentiation and epiblast proliferation. Although many aspects of the BORCS6 mutant phenotype may be cell-autonomous, such as increased cellular and nuclear size, the significant epiblast lineage reduction, even though BORCS6 is not robustly expressed in epiblast cells, suggests a perturbation of cell-cell communication in mutant embryos. Taken together, our results support an essential role for lysosomal function both in cellular health and the paracrine developmental signaling processes that prepare the early egg cylinder to initiate gastrulation.

Conclusion

Proper lysosomal function is essential for cellular health. In a rapidly changing environment such as the early mammalian embryo, macromolecules must be degraded efficiently to enable the cellular remodeling necessary for differentiation. Eliminating BORCS6 function elicits both a cellular phenotype and an embryonic patterning defect. Borcs6-null embryos contain fewer and larger cells than control littermates, characterized by large nuclei, accumulation of late endosomes, and improper dispersal of lysosomes. At embryonic day 6.5, mutant embryos lack the cellular organization of littermate controls, with a much smaller epiblast and obviously dysmorphic visceral endoderm cells. Endocytosis is unaffected in Borcs6-null embryos, but late endosomes appear unable to efficiently fuse with lysosomes for degradation in null cells. These results expand our understanding of the critical role degradative pathways play during early mammalian development.

Methods

Animals

The *Borcs6* knockout was generated by Jackson Laboratories (*Borcs6*^{tm1.1(KOMP)Vlcr}, JAX-12882A-F6-1). 1095 base pairs of the *Borcs6* genomic sequence were replaced with the *lacZ* reporter gene sequence, removing part of exon 1 in the C57BL/6NJ background.

Embryo retrieval and genotyping

Borcs6-null embryos were generated by heterozygote intercrosses. Males and females were housed together, and the presence of a vaginal plug defined E0.5. All embryos were genotyped by PCR using primers (given 5' to 3'): wild type (AGCTGACAGCGTTGAGTGTG and TCCTACTGGACCCTGGTCTG; 268 bp) and knockout (CGGTCGCTACCATTACCAGT and TCCTACTGGACCCTGGTCTG; 484 bp).

All results presented were performed on at least 3 mutant embryos (often more). All experiments were approved by the University of Massachusetts Amherst Institutional Animal Care and Use Committee.

RNA extraction and RT-PCR analysis

RNA was extracted using the Zymo Research Quick DNA/RNA Microprep Plus Kit (D7005). cDNA synthesis was performed using Bio-Rad iScript cDNA Synthesis (Bio-Rad, 1708890). RT-PCR was performed for 35 cycles of 30 seconds at 60°C, 72°C and 95°C with the following primers with indicated gene names unless otherwise specified (given 5' to 3'): *Borcs6* (399 bp): (CTGGACACTTGGGAGGACAA and GCTCTAGGGGGCTGGAGATA); *Mtp117* (414 bp): (CCATCTGCTGCGGAAGTTG and CTTGCGTCCTGGTTATGGTG); *Wnt3* (649 bp): (CAGCGTAGCAGAAGGTGTGA and AAAGTTGGGGGAGTTCTCGT); *Hhex* (401 bp): (CCTCTGCACAAAAGGAAAGG and TAGCCTTTATCCCCCTCGAT); *Eomes* (451 bp): (GGCAAAGCGGACAATAACAT and GACCTCCAGGGACAATCTGA); *Cer1* (493 bp): (CAGGCTTGAAGATTCTGGA and CGTCTTCACCATGCACTGAC); *Brachury* (313 bp): (CAIGTACTCTTTCTTGCTGG and GGTCTCGGGAAAGCAGTGGC).

Sectioned in situ hybridization

Protocol is adapted from Wang et al., 2015. Freshly dissected embryos in decidua were fixed in 4% paraformaldehyde (PFA) overnight, dehydrated in ethanol, cleared in xylene, embedded with paraffin, and sectioned at 7µm thick. Sections were deparaffinized and rehydrated, then fixed in 4% PFA and washed in Proteinase K. Proteinase K was deactivated by washing in glycine, and slides were fixed in 4% PFA once more. Sections were washed in 0.25% acetic anhydride in 0.1M triethanolamine, then incubated at 65°C in hybridization buffer before incubating with an antisense RNA probe overnight at 70°C. Next, sections were washed in solutions containing formamide, SSC, and SDS, followed by a final wash in maleic acid buffer (MAB) containing maleic acid, 5M NaCl, NaOH, and Tween-20. Blocking was performed in MAB with 2% Boehringer block. Embryos were incubated with an antibody solution containing Anti-Digoxigenin-AP (1:5,000, Roche Diagnostics, 11093274910) and heat inactivated sheep serum (Sigma-Aldrich, S2263) for 2 hours. Sections were washed four times in MABT buffer, then three times in NTMT containing 0.1M NaCl, 0.1M Tris base, 0.05M MgCl₂, and 1% Tween-20. Slides were stained in BM purple (Roche Diagnostics, 11442074001) for 4 days and staining was stopped in 1mM EDTA/PBT. Sections were once again dehydrated and counterstained in Eosin Y (Polysciences, Inc.), coverslipped with Cytoseal 60, and imaged.

X-gal (5-bromo-4-chloro-3-indolyl-β-D-galactopyranoside) staining

Freshly dissected embryos were fixed in X-gal buffer containing 0.2% glutaraldehyde and 1% formaldehyde on ice for 15 minutes and subjected to a modified protocol from Tremblay *et al.*, (2000). Fixed embryos were washed with X-gal buffer (PBS, 5mM EGTA, 2mM MgCl₂·6H₂O, 0.2% NP-40, 0.2mM deoxycholate) for 10 minutes, three times, and stained with X-gal stain (X-gal buffer, 5 mM potassium ferricyanide and 5 mM potassium ferrocyanide and 0.5 mg/ml X-gal) overnight at 37°C. Embryos were then dehydrated in ethanol, cleared in xylene, embedded with paraffin and sectioned at 7µm thick. The

sectioned embryos were deparaffinized and rehydrated for subsequent processing. Eosin staining was performed by immersing rehydrated sectioned embryos in eosin for 15 seconds, followed by 95% ethanol washes for 2 minutes, 100% ethanol for 2 minutes, and lastly cleared in xylene. Slides were then sealed with Cytoseal 60. X-gal-stained sections were imaged with a Nikon Ti2 Eclipse inverted microscope.

In some instances, embryos were stained using a Beta-galactosidase staining kit (BioVision, K802). Freshly dissected embryos were fixed in the fixing solution for 15 minutes over ice, then washed twice in PBS for 15 minutes at room temperature. Embryos were stained overnight in staining solution as described in the kit protocol. Embryos were washed once in PBS for 10 minutes at room temperature, then fixed in 4% PFA for one hour at room temperature. Embryos were then dehydrated, embedded, and counterstained as described above.

Whole-mount in situ hybridization

Freshly dissected embryos were fixed in 4% paraformaldehyde for 2–4 hours on ice and subjected to WISH (Tremblay et al., 2001). Embryos were dehydrated in methanol and stored up to 1 month. Embryos were rehydrated in a series of methanol washes in PBT. Subsequently, the embryos were rinsed twice in PBT for 5 minutes and bleached in 6% hydrogen peroxide for 1 hour. Embryos were then rinsed with PBT, treated with Proteinase K for 6–8 minutes and incubated with glycine in PBT for 5 minutes. After rinsing twice with PBT for 5 minutes, embryos were fixed with 4% paraformaldehyde with 0.02% glutaraldehyde for 20 minutes. Embryos were rinsed twice in PBT for 5 minutes and incubated in 1:1 hybridization buffer/PBT for 10 minutes and subsequently in hybridization buffer for 10 minutes. Embryos were then incubated with 150ng RNA probes in hybridization buffer at 70°C overnight. The next day, embryos were washed with solutions containing formamide, 20X SSC, 1M citric acid, 20% SDS and Tween 20 for 30 minutes at 70°C for the first three washes, and at 65°C for the last three washes. Following this step, the embryos were rinsed in maleic acid buffer (MAB) for 5 minutes, three times. The embryos were then blocked in MAB with 2% Boehringer block for 1 hour at room temperature and then incubated with the antibody solution containing Anti-Digoxigenin-AP (1:2,000, Roche Diagnostics, 11093274910), heat inactivated sheep serum (Sigma-Aldrich, S2263) and levamisole (Sigma-Aldrich, L9756) at 4°C overnight. The following day, the embryos were washed six times with MAB for at least 1 hour. The embryos were then rinsed with alkaline phosphatase buffer containing 1M Tris-HCl pH 9.5, 5M NaCl, 1M MgCl₂ and Tween 20 for 10 minutes, three times, and developed in BM purple solution (Roche Diagnostics, 11442074001) until the color has developed. The embryos were then washed with 2mM EDTA/PBT, fixed in 4% paraformaldehyde overnight, washed twice in PBT, and imaged.

Borcs6 probe: Chr. 11 68951023 to 68951322

Hematoxylin and Eosin staining (H&E)

Freshly dissected embryos were fixed in 4% paraformaldehyde overnight, dehydrated in ethanol, cleared in xylene, embedded with paraffin and sectioned at 7µm, as previously

described (Wallingford et al., 2013). The sectioned embryos were deparaffinized and rehydrated for subsequent procedures. Slides were then stained with hematoxylin for 45 seconds, placed under gently running tap water for 1 minute, submerged in Scott's Tap Water Substitute (20 h MgSO₄, 3.5g NaHCO₂/L dH₂O) for 1 minute, and then washed in still tap water for another minute. The slides were quickly dipped into 95% ethanol, stained with eosin for 15 seconds, and then again washed in 95% ethanol with two 2-minute washes in 100% ethanol. Lastly, the slides were washed with xylenes three times for one minute each, and then sealed with Cytoseal 60. H&E-stained sections were imaged with a Nikon Ti2 Eclipse inverted microscope.

Paraffin embedding and section immunofluorescence (IF)

Freshly dissected embryos were fixed in 4% paraformaldehyde overnight, dehydrated in ethanol, cleared in xylene, embedded with paraffin, and sectioned at 7µm thick. The sectioned embryos were deparaffinized and rehydrated for subsequent procedures. Antigen retrieval was performed by boiling the slides in citric acid buffer (pH 6) for 4 minutes and cooling to room temperature. The slides were then rinsed twice in phosphate buffered saline/0.01% Tween 20 (PBT) for 2 minutes and blocked with 0.5% milk in PBT for 2 hours at room temperature in a humid chamber. Primary antibodies were applied in 0.05% milk/PBT and incubated at 4°C overnight in a humid chamber. The slides were then rinsed three times with PBT for 15 minutes, followed by incubation with secondary antibodies at room temperature for 1 hour in a humid chamber. Next, the slides were rinsed with PBS for 15 minutes, three times. Nuclei were counterstained with DAPI (4',6-diamidino-2-phenylindole) in PBS (1:10,000) for 3 minutes. Slides were rinsed with 1X PBS and sealed with ProLong Gold (Thermo Fisher Scientific, P36934). Fluorescent slides were imaged with a Nikon Ti2 Eclipse inverted microscope. The primary antibodies used and their dilution include: E-cadherin (BD Biosciences, 610181, 1:500); Cdx2 (Abcam, ab76541, 1:1000); Oct4 (Abcam, ab27985, 1:200); Rab7 (Cell Signaling Technology, #9367, 1:200); Lamp1 (Abcam, ab25245, 1:200).

The secondary antibodies used include: Alexa Fluor 488 donkey anti-mouse (Thermo Fisher Scientific, A21202, 1:500); Alexa Fluor 546 donkey anti-rabbit (Thermo Fisher Scientific, A10040, 1:500); Alexa Fluor Plus 647 donkey anti-rat (Thermo Fisher Scientific, A48272, 1:500); Alexa Fluor 647 donkey anti-goat (Thermo Fisher Scientific, A21447, 1:500); DAPI (Molecular Probes, 1:10,000). Slides were imaged with a Nikon Ti2 Eclipse inverted microscope.

TUNEL staining

Embryos were fixed, dehydrated, cleared, embedded, and sectioned as described above. Staining was carried out using the TUNEL Assay kit – HRP-DAB from Abcam (ab206386), following manufacturer's protocol. Significance was calculated using Fisher's Exact Test of Independence.

Whole-mount immunofluorescence (WMIF)

Whole-mount immunofluorescence was conducted on embryos as described in *Manipulating the Mouse Embryo* (Behringer et al., 2014). Freshly dissected embryos were fixed in 4%

paraformaldehyde at 4°C overnight. The embryos were washed in cold PBS, digested in 50 µg/mL Proteinase K, washed in cold PBS again, and dehydrated in methanol. The embryos were then bleached overnight in MeOH:H₂O₂ (4:1) at 4°C. Next, embryos were rehydrated and blocked in PBS with 1% BSA and 11% sucrose. Embryos were incubated overnight at 4°C in diluted primary antibody in the blocking solution. The following day, embryos were washed three times in PBS for 2 hours before incubating overnight at 4°C in diluted secondary antibody in the blocking solution. Embryos were again washed three times for 2 hours in PBS. Nuclei were stained with DAPI (4',6-diamidino-2-phenylindole) in PBS (1:10,000) for 10 minutes. Embryos were washed for 5 minutes in PBS, then imaged with a Nikon Eclipse Ti Series inverted microscope with a C2 confocal attachment.

The primary antibodies used and their dilution include: Rab7 (Cell Signaling Technology, #9367, 1:200); Lamp1 (Abcam, ab25245, 1:200).

The secondary antibodies used include: Alexa Fluor 546 donkey anti-rabbit (Thermo Fisher Scientific, A10040, 1:500); Alexa Fluor Plus 647 donkey anti-rat (Thermo Fisher Scientific, A48272, 1:500); DAPI (Molecular Probes, 1:10,000).

Measurements

Immunofluorescence was conducted on sagittal sectioned mutant E6.5 embryos and control littermates using Cdx2 and Oct4 to mark the extraembryonic ectoderm and epiblast, respectively. Thickness of the visceral endoderm surrounding the extraembryonic ectoderm was measured in 3 locations and averaged for each embryo. Thickness of the visceral endoderm surrounding the epiblast was also measured in 3 locations and averaged for each embryo. Height of extraembryonic ectoderm was defined as the distance from the most proximal Cdx2-positive cell to the most distal Cdx2-positive cell. Height of epiblast was defined as the distance from the most proximal Oct4-positive cell to the most distal Oct4-positive cell. These measurements were divided to produce the ratio of epiblast to extraembryonic ectoderm. For epiblast cell area, 10 to 20 Oct4-positive cells were measured per embryo. 20 to 30 Cdx2-positive cells per embryo were measured for extraembryonic ectoderm cell area. Nucleus area was measured in 30 cells per embryo. Measurements were taken using the NIS Analysis software. For cell counting, nuclei were counted on every third 7 µm section throughout the entirety of each embryo (3 control E6.5, 4 E6.5 mutants, and 2 control E5.5 embryos). Significance was calculated using a two-tailed Student's t test.

Embryo culture and dextran uptake assessment

Embryos were dissected into media containing 89% DMEM (Lonza, 12-707F), 10% FBS, 0.5% Glutamax (Gibco, 35050-061) and 0.5% penicillin/streptomycin. Adapted from Aoyama et al. (2012), embryos were moved into the same media containing 0.5 mg/mL dextran Alexa Fluor 647 (Thermo Fisher Scientific, D22914) and incubated for 10 minutes at 37°C, 5% CO₂, 5% O₂. Embryos were washed in media twice, then incubated in media again. Images were taken 10 minutes after dextran-647, 45 minutes, and 65 minutes. Embryos were fixed in 4% PFA overnight at 4°C before whole-mount immunofluorescence was conducted.

Acknowledgements

We would like to thank members of the Mager and Tremblay labs for providing useful input throughout the project. We would also like to thank George W. Bell for his statistical input. This work was supported by R01HD083311 to JM.

References

- Almacellas E, Pelletier J, Day C, Ambrosio S, Tauler A, & Mauvezin C (2021). Lysosomal degradation ensures accurate chromosomal segregation to prevent chromosomal instability. *Autophagy*, 17(3), 796. 10.1080/15548627.2020.1764727 [PubMed: 32573315]
- Aoyama M, Sun-Wada GH, Yamamoto A, Yamamoto M, Hamada H, & Wada Y (2012). Spatial Restriction of Bone Morphogenetic Protein Signaling in Mouse Gastrula through the mVam2-Dependent Endocytic Pathway. *Developmental Cell*, 22(6), 1163–1175. 10.1016/j.devcel.2012.05.009 [PubMed: 22698281]
- Arnold SJ, & Robertson EJ (2009). Making a commitment: cell lineage allocation and axis patterning in the early mouse embryo. *Nature Reviews Molecular Cell Biology* 2009 10:2, 10(2), 91–103. 10.1038/nrm2618 [PubMed: 19129791]
- Ballabio A, & Bonifacino JS (2020). Lysosomes as dynamic regulators of cell and organismal homeostasis. In *Nature Reviews Molecular Cell Biology* (Vol. 21, Issue 2, pp. 101–118). Nature Research. 10.1038/s41580-019-0185-4 [PubMed: 31768005]
- Cabukusta B, & Neefjes J (2018). Mechanisms of lysosomal positioning and movement. In *Traffic* (Vol. 19, Issue 10, pp. 761–769). Blackwell Munksgaard. 10.1111/tra.12587 [PubMed: 29900632]
- De Pace R, Britt DJ, Mercurio J, Hoffmann V, Abebe D, Bonifacino Correspondence JS, Foster AM, Djavaherian L, & Bonifacino JS (2020). Synaptic Vesicle Precursors and Lysosomes Are Transported by Different Mechanisms in the Axon of Mammalian Neurons. *CellReports*, 31, 107775. 10.1016/j.celrep.2020.107775
- Dickinson ME (2016). High-throughput discovery of novel developmental phenotypes. *Nature*, 537, 508–514. <https://www.mousephenotype.org/data/genes/MGI:1919618> [PubMed: 27626380]
- Falcón-Pérez JM, Starcevic M, Gautam R, & Dell'Angelica EC (2002). BLOC-1, a novel complex containing the pallidin and muted proteins involved in the biogenesis of melanosomes and platelet-dense granules. *The Journal of Biological Chemistry*, 277(31), 28191–28199. 10.1074/JBC.M204011200 [PubMed: 12019270]
- Garg S, Sharma M, Ung C, Tuli A, Barral DC, Hava DL, Veerapen N, Besra GS, Hacohen N, & Brenner MB (2011). Lysosomal Trafficking, Antigen Presentation, and Microbial Killing Are Controlled by the Arf-like GTPase Arl8b. *Immunity*, 35(2), 182–193. 10.1016/J.IMMUNI.2011.06.009 [PubMed: 21802320]
- Holdgaard SG, Cianfanelli V, Pupo E, Lambrughli M, Lubas M, Nielsen JC, Eibes S, Maiani E, Harder LM, Wesch N, Foged MM, Maeda K, Nazio F, de la Ballina LR, Dötsch V, Brech A, Frankel LB, Jäättelä M, Locatelli F, ... Cecconi F (2019). Selective autophagy maintains centrosome integrity and accurate mitosis by turnover of centriolar satellites. *Nature Communications* 2019 10:1, 10(1), 1–19. 10.1038/s41467-019-12094-9
- Huotari J, & Helenius A (2011). Endosome maturation. *The EMBO Journal*, 30(17), 3481. 10.1038/EMBOJ.2011.286 [PubMed: 21878991]
- Jia R, Guardia CM, Pu J, Chen Y, & Bonifacino JS (2017). BORC coordinates encounter and fusion of lysosomes with autophagosomes. *Autophagy*, 13(10), 1648–1663. 10.1080/15548627.2017.1343768 [PubMed: 28825857]
- Jullien J, & Gurdon J (2005). Morphogen gradient interpretation by a regulated trafficking step during ligand-receptor transduction. 10.1101/gad.341605
- Kawamura N, Sun-Wada GH, Aoyama M, Harada A, Takasuga S, Sasaki T, & Wada Y (2012). Delivery of endosomes to lysosomes via microautophagy in the visceral endoderm of mouse embryos. *Nature Communications*, 3(1), 1–10. 10.1038/ncomms2069
- Khatter D, Raina VB, Dwivedi D, Sindhwani A, Bahl S, & Sharma M (2015). The small GTPase Arl8b regulates assembly of the mammalian HOPS complex on lysosomes. *Journal of Cell Science*, 128(9), 1746–1761. 10.1242/JCS.162651 [PubMed: 25908847]

- Korolchuk VI, Saiki S, Lichtenberg M, Siddiqi FH, Roberts EA, Imarisio S, Jahreiss L, Sarkar S, Futter M, Menzies FM, O’Kane CJ, Deretic V, & Rubinsztein DC (2011). Lysosomal positioning coordinates cellular nutrient responses. *Nature Cell Biology*, 13(4), 453–462. 10.1038/ncb2204 [PubMed: 21394080]
- Matteoni R, & Kreis TE (n.d.). Translocation and Clustering of Endosomes and Lysosomes Depends on Microtubules.
- Niwa S, Tao L, Lu SY, Liew GM, Feng W, Nachury MV, & Shen K (2017). BORG Regulates the Axonal Transport of Synaptic Vesicle Precursors by Activating ARL-8. *Current Biology*, 27(17), 2569–2578.e4. 10.1016/j.cub.2017.07.013 [PubMed: 28823680]
- Orr A, Song H, Rusin SF, Kettenbach AN, & Wickner W (2017). HOPS catalyzes the interdependent assembly of each vacuolar SNARE into a SNARE complex. *Molecular Biology of the Cell*, 28(7), 975. 10.1091/MBC.E16-10-0743 [PubMed: 28148647]
- Perera RM, & Zoncu R (2016). The Lysosome as a Regulatory Hub. *Annu. Rev. Cell Dev. Biol*, 32, 223–253. 10.1146/annurev-cellbio-111315-125125 [PubMed: 27501449]
- Power MA, & Tam PPL (1993). Onset of gastrulation, morphogenesis and somitogenesis in mouse embryos displaying compensatory growth. *Anatomy and Embryology*, 187(5), 493–504. 10.1007/BF00174425 [PubMed: 8342794]
- Pu J, Schindler C, Jia R, Jarnik M, Backlund P, & Bonifacino JS (2015). BORG, a Multisubunit Complex that Regulates Lysosome Positioning. *Developmental Cell*, 33(2), 176–188. 10.1016/j.devcel.2015.02.011 [PubMed: 25898167]
- Snouwaert JN, Church RJ, Jania L, Nguyen MT, Wheeler ML, Saintsing A, Mieczkowski P, Manuel de Villena FP, Armao D, Moy SS, Lorenzo DN, & Koller BH (2018). A Mutation in the Borsc7 Subunit of the Lysosome Regulatory BORG Complex Results in Motor Deficits and Dystrophic Axonopathy in Mice. *Cell Reports*, 24(5), 1254–1265. 10.1016/j.celrep.2018.06.118 [PubMed: 30067980]
- Tian JH, Wu ZX, Unzicker M, Lu L, Cai Q, Li C, Schirra C, Matti U, Stevens D, Deng C, Rettig J, & Sheng ZH (2005). The role of snapin in neurosecretion: Snapin knock-out mice exhibit impaired calcium-dependent exocytosis of large dense-core vesicles in chromaffin cells. *Journal of Neuroscience*, 25(45), 10546–10555. 10.1523/JNEUROSCI.3275-05.2005 [PubMed: 16280592]
- Tremblay KD, Dunn NR, & Robertson EJ (2001). Mouse embryos lacking Smad1 signals display defects in extra-embryonic tissues and germ cell formation. *Development*, 128(18), 3609–3621. 10.1242/DEV.128.18.3609 [PubMed: 11566864]
- Tremblay KD, Hoodless PA, Bikoff EK, & Robertson EJ (2000). Formation of the definitive endoderm in mouse is a Smad2-dependent process. *Development (Cambridge, England)*, 127(14), 3079–3090. 10.1242/dev.127.14.3079
- Wada Y (2013). Vacuoles in mammals: A subcellular structure indispensable for early embryogenesis. *Bioarchitecture*, 3(1), 13. 10.4161/BIOA.24126 [PubMed: 23572040]
- Wada Y, Sun-Wada GH, & Kawamura N (2013). Microautophagy in the visceral endoderm is essential for mouse early development. In *Autophagy* (Vol. 9, Issue 2, pp. 252–254). Taylor and Francis Inc. 10.4161/auto.22585 [PubMed: 23108279]
- Wallingford MC, Angelo JR, & Mager J (2013). Morphogenetic analysis of peri-implantation development. *Developmental Dynamics: An Official Publication of the American Association of Anatomists*, 242(9), 1110–1120. 10.1002/DVDY.23991 [PubMed: 23728800]
- Wang J, Rhee S, Palaria A, & Tremblay KD (2015). FGF signaling is required for anterior but not posterior specification of the murine liver bud. *Developmental Dynamics*, 244(3). 10.1002/dvdy.24215
- Xu H, & Ren D (2015). *Lysosomal Physiology*. 10.1146/Annurev-Physiol-021014-071649, 77, 57–80. 10.1146/ANNUREV-PHYSIOL-021014-071649
- Yang Q, He X, Yang L, Zhou Z, Cullinane AR, Wei A, Zhang Z, Hao Z, Zhang A, He M, Feng Y, Gao X, Gahl WA, Huizing M, & Li W (2012). The BLOS1-Interacting Protein KXD1 is Involved in the Biogenesis of Lysosome-Related Organelles. *Traffic*, 13(8), 1160–1169. 10.1111/j.1600-0854.2012.01375.x [PubMed: 22554196]
- Zhang A, He X, Zhang L, Yang L, Woodman P, & Li W (2014). Biogenesis of lysosome-related organelles complex-1 subunit 1 (BLOS1) interacts with sorting nexin 2 and the endosomal

sorting complex required for transport-I (ESCRT-I) component TSG101 to mediate the sorting of epidermal growth factor receptor into endo. *Journal of Biological Chemistry*, 289(42), 29180–29194. 10.1074/jbc.M114.576561 [PubMed: 25183008]

Zhou W, He Q, Zhang C, He X, Cui Z, Liu F, & Li W (2016). BLOS2 negatively regulates notch signaling during neural and hematopoietic stem and progenitor cell development. *ELife*, 5(OCTOBER2016). 10.7554/eLife.18108

Author Manuscript

Author Manuscript

Author Manuscript

Author Manuscript

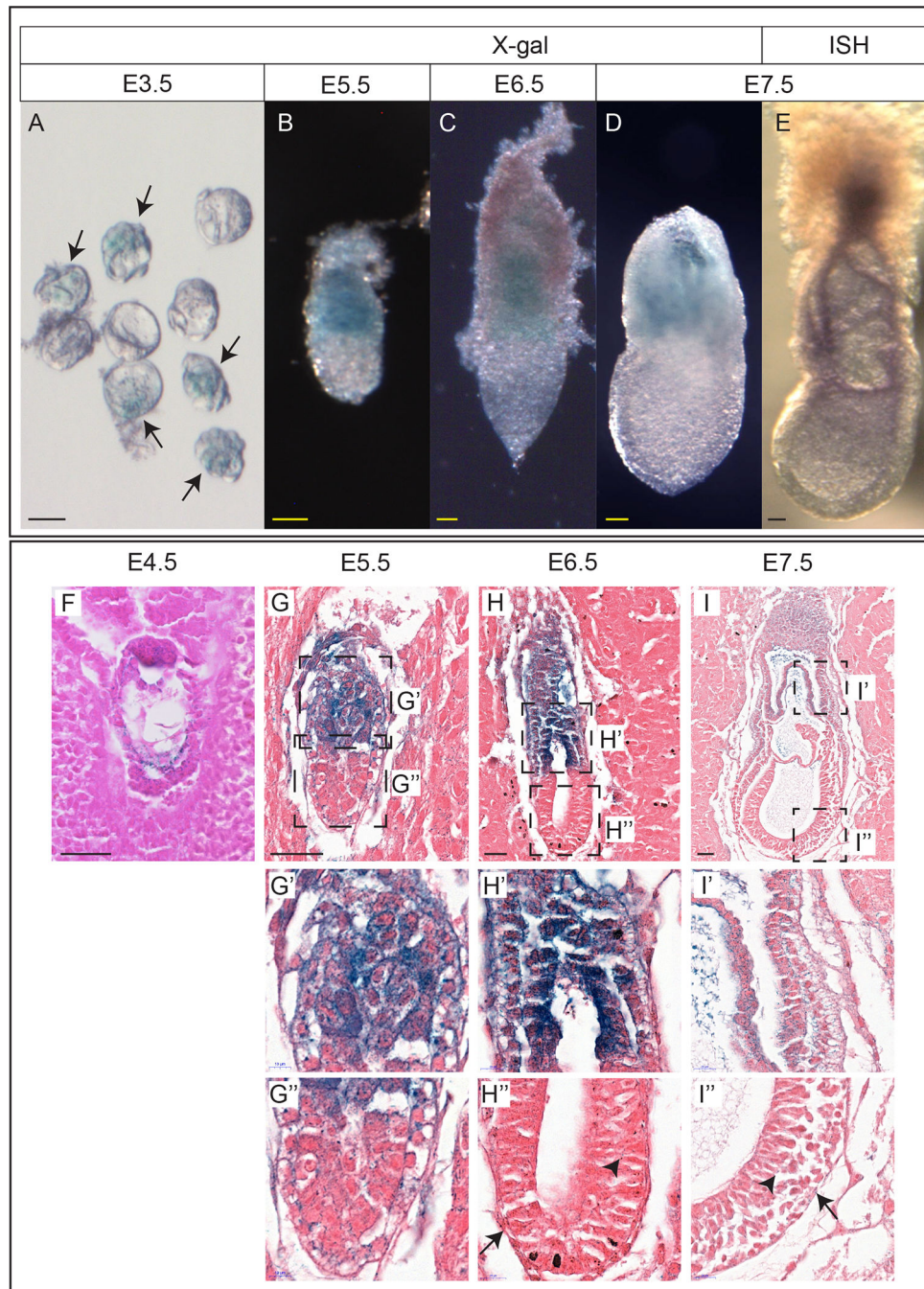


Figure 1: Expression of BORCS6 during early development.

(A) A litter of heterozygous and wildtype blastocysts after X-gal staining. Arrows indicate heterozygous embryos. (B-D) Heterozygous E5.5(B) E6.5(C) and E7.5(D) embryos after X-gal staining. (E) Wildtype E7.5 embryo after *in situ* hybridization using a probe against *Borcs6*. (F) Sagittal section of a heterozygous E4.5 embryo in decidua after staining with X-gal. (G) Sagittal section of a heterozygous E5.5 embryo in decidua after staining with X-gal. Insets in (G) are magnified in (G') and (G''). (H) Sagittal section of a heterozygous E6.5 embryo in decidua after staining with X-gal. Insets in (H) are magnified in (H')

and (H''). Arrow indicates staining in the distal half of the visceral endoderm. Arrowhead indicates staining in epiblast. (I) Sagittal section of a heterozygous E7.5 embryo in decidua after staining with X-gal. Insets in (I) are magnified in (I') and (I''). Arrow indicates staining in the visceral endoderm. Arrowhead indicates staining in epiblast.

Scale bar: 50 μ m

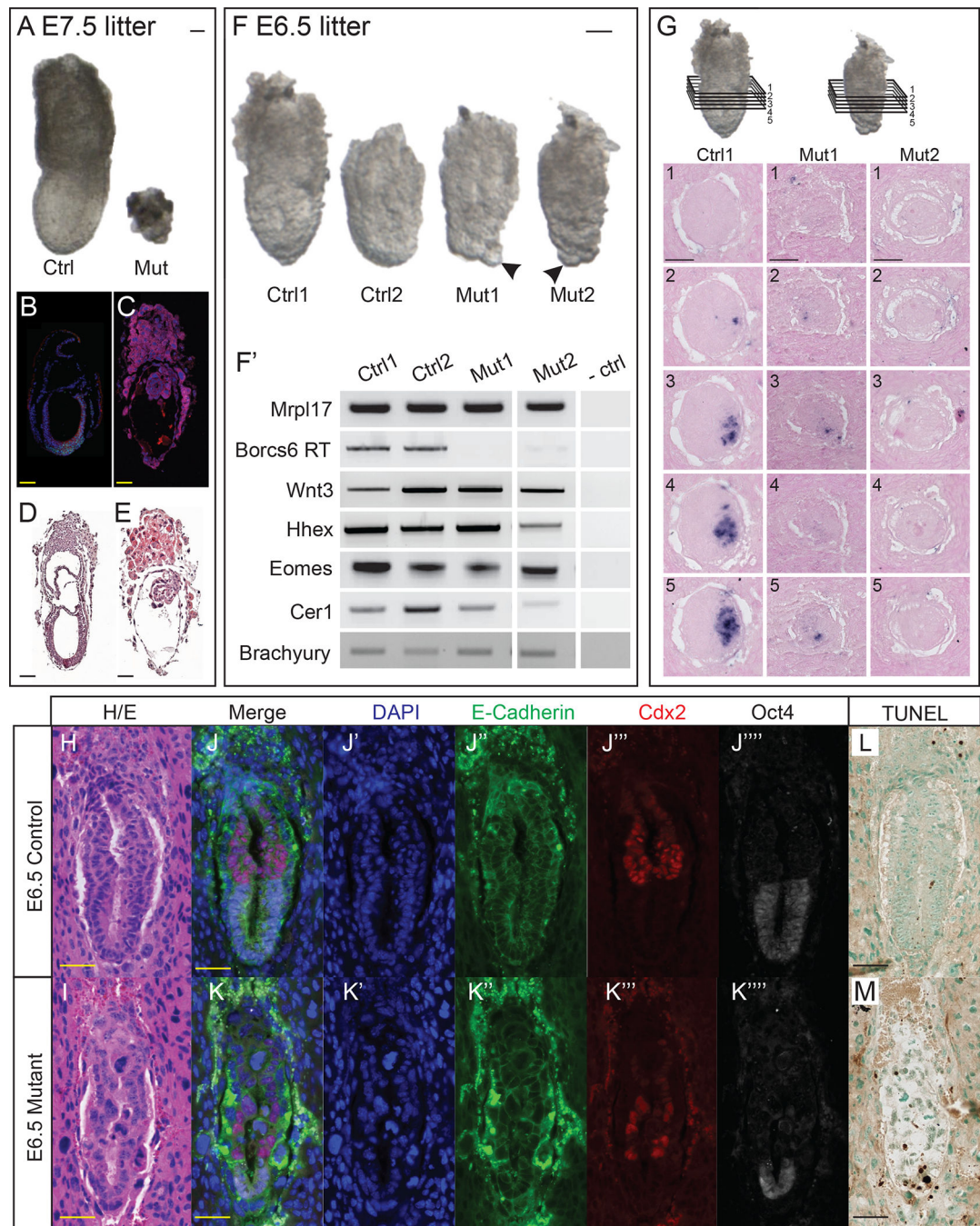


Figure 2: BORCS6 mutant embryos are present but defective at E6.5 and E7.5.

(A) Control and mutant littermates from a heterozygous intercross retrieved at embryonic day 7.5 (B, C) Immunofluorescence conducted on E7.5 wildtype and mutant embryos, respectively, using DAPI to stain nuclei (blue) and antibodies against E-cadherin (red) and Brachyury (green). (D, E) Hematoxylin and eosin-stained E7.5 wildtype and mutant embryos, respectively. (F) Control and mutant littermates from a heterozygous intercross retrieved at E6.5. Arrows indicate large embryonic visceral endoderm cells in $-/-$ embryos. (F') RT-PCR panel for embryos seen in (F). (G) Schematic of transverse sections

analyzed for expression of *Brachyury* in E6.5 wildtype and mutant embryos. Insets 1–5 are consecutive transverse sections of embryos in decidua stained for *Brachyury* transcripts by *in situ* hybridization from wildtype (Ctrl1) and mutant (Mut1, Mut2) embryos. (H, I) Hematoxylin and eosin-stained wildtype and mutant embryo, respectively. (J, K) Immunofluorescence conducted on wildtype and mutant embryos using DAPI to counterstain nuclei (J', K'), and antibodies against E-cadherin (J'', K''), Cdx2 (J''', K'''), and Oct4 (J''', K'''). Note H and J, and I and K are the very same embryo section images after subsequent IF/HE protocols. (L, M) TUNEL-stained wildtype and mutant E6.5 embryos, with methyl green counterstain. TUNEL-positive nuclei are stained dark brown. Scale bar: 50 μ m

Author Manuscript

Author Manuscript

Author Manuscript

Author Manuscript

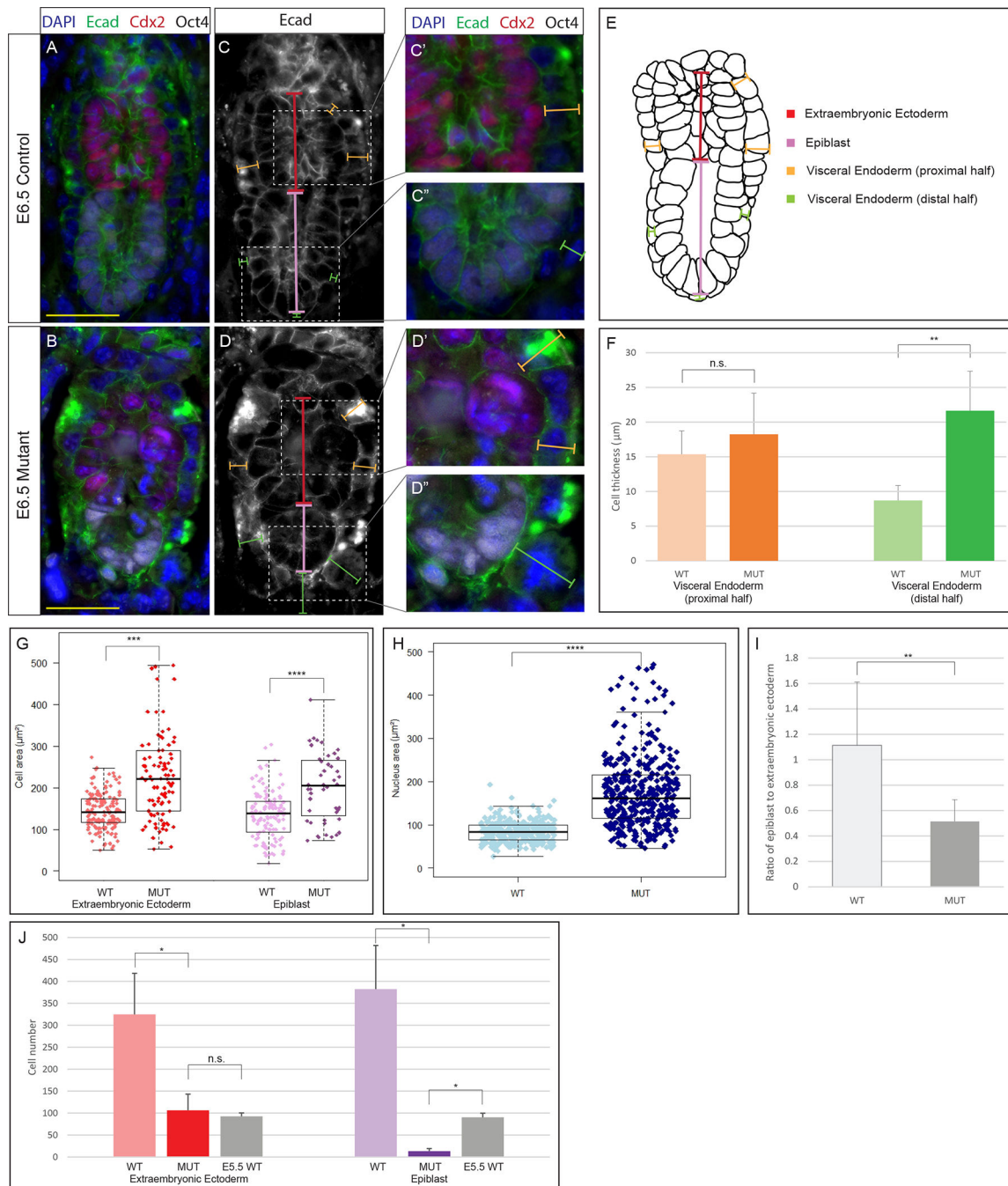


Figure 3: Morphological defects in BORCS6 mutant embryos.

IF analysis of E-cadherin (green), Cdx2 (red), Oct4 (white) and DAPI (blue) on wildtype (A) and mutant (B) embryos. Scale bar: 50 μm . Measurements taken (C-D), including VE-extraembryonic (orange), VE-epiblast (green), extraembryonic ectoderm height (red), and epiblast height (purple). Insets show magnified region with merged immunofluorescence for C (C', C'') and D (D', D''). (E) Schematic of measurements taken (10 littermate and 12 mutant embryos). (F) Average cell thickness of VE-proximal half (orange) and VE-distal half (green). The distal part of the visceral endoderm is thicker in mutant embryos

than wildtype embryos ($p = 0.0012$). (G) Box-and-whisker plot comparing cell areas in wildtype and mutant extraembryonic ectoderm (red) and epiblast (purple). Cells were larger in mutant extraembryonic ectoderm ($p < 0.0001$) and mutant epiblast ($p = 0.001$). (H) Box-and-whisker plot comparing area of nuclei in mutant embryos and control littermates. Nuclei are larger throughout mutant embryos than in control littermates ($p < 0.0001$). (I) Ratio of epiblast/extraembryonic ectoderm is smaller than control ratio ($p = 0.0016$). (J) Lineage specific cell numbers compared between E6.5 control, E6.5 mutant, and E5.5 control embryos. Mutant embryos had fewer epiblast cells than E6.5 and E5.5 control embryos ($p < 0.05$).

Statistical significance was calculated by two-tailed Student's t test. Error bars represent standard deviation. * $p < 0.05$, ** $p < 0.01$, *** $p < 0.001$, **** $p < 0.0001$.

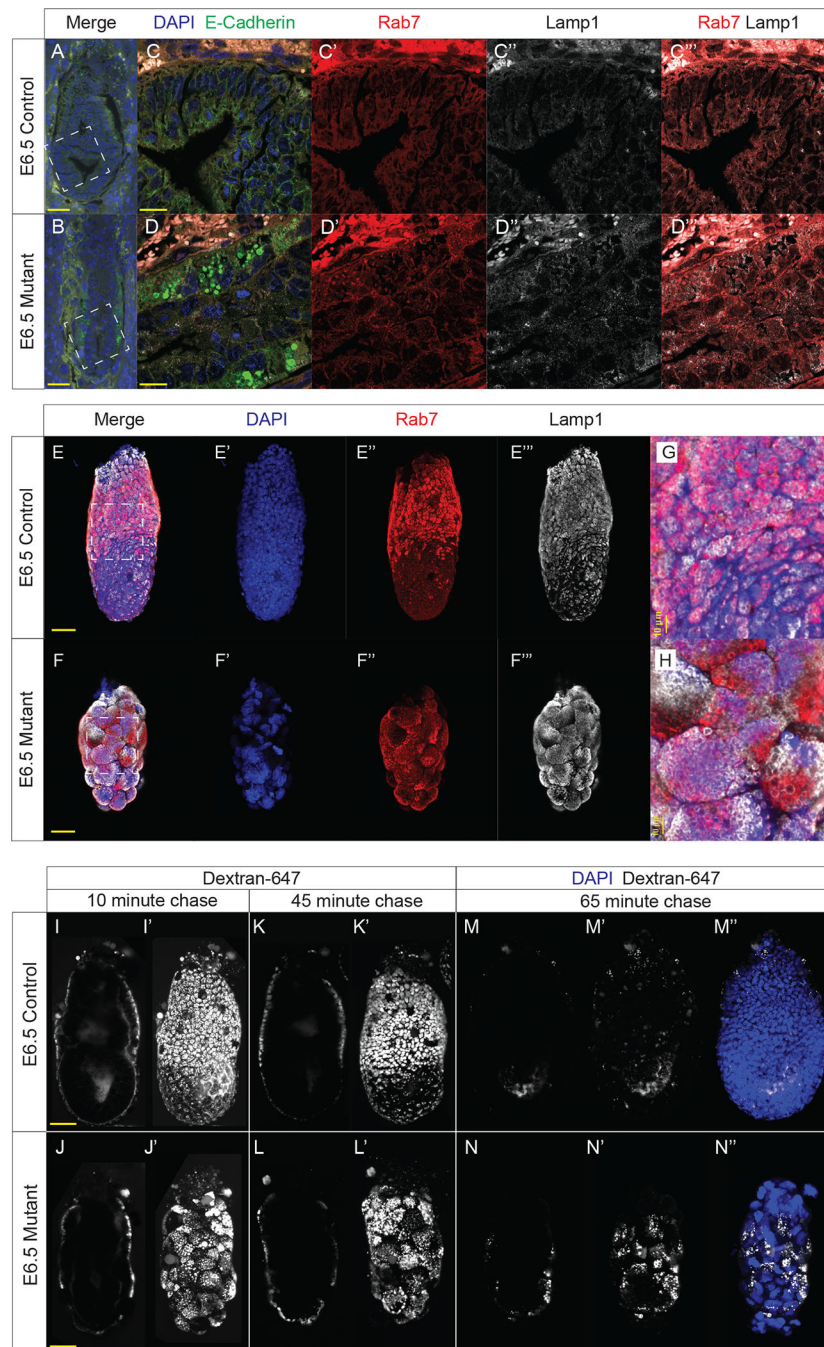


Figure 4: Borcs6 is necessary for proper endo-lysosomal function in the developing embryo. IF analysis of E-cadherin (green), Rab7 (red), Lamp1 (white) and nuclei counterstained with DAPI (blue) in E6.5 control littermate (A) and mutant embryo (B) (scale bar: 50 μ m). Insets in (A) and (B) are magnified in (C) and (D), respectively (scale bar: 20 μ m). Individual channels are shown for Rab7 (C', D'), and Lamp1 (C'', D''). (C''') and (D''') show a merged image of Rab7 and Lamp1.

(E-E''' and F-F''') Maximum intensity projections of confocal images illustrate localization of Rab7 (red), Lamp1 (white) and nuclei stained with DAPI (blue) in control and mutant E6.5 embryos (scale bar: 50 μ m). Inset boxes are magnified in (G) and (H).

Sagittal optical section illustrating internalization of dextran-647 (white) in control (I) and mutant (J) embryos after 10-minute wash in the absence of dextran-647. Maximum intensity projections are shown in (I') and (J'). Images were also collected after 45-minute incubation in the absence of dextran-647 (K-K', L-L'). After 65 minutes of incubation, embryos were fixed, and immunofluorescence was conducted. Optical sections of the dextran are shown in (M) and (N), while maximum intensity projection is depicted in (M') and (N'), respectively. (M'') and (N'') are maximum intensity projections with both dextran (white) and nuclei counterstained with DAPI (blue). Scale bar: 50 μ m